

Flow Mode Dependent Partitioning Processes of Preferential Flow Dynamics in Unsaturated Fractures - Findings From Analogue Percolation Experiments

I. Introduction

Free-surface flow at fracture intersections

- gravity driven free-surface flow has been identified and described in flow visualization experiments (e.g. Towell (1966); Schmucki (1990); Podgorski (2001))
- experimental approaches using analogue fracture networks suggest the occurrence of versatile flow dynamics during infiltration in the fractured vadose zone (e.g. Dragila (2003, 2004); Glass (2003); Ghezzehei (2005); Nicholl (2005))
- field studies indicate the existence of preferential flow paths in unsaturated conditions (Nimmo (2012)), which numerical approaches recreating flow and transport fail to recover due to the non-linear nature of mass partitioning processes

Objective

- develop and apply methods to accurately delineate droplet and rivulet flow in analogue fracture percolation experiments
- identify the effects of variable flow regimes on mass travel time distribution
- investigate the impacts of variable fracture geometry on partitioning dynamics at unsaturated fracture intersections
- employ an analytical solution proposed by Kordilla et al. (2017) to describe capillary driven fracture inflow

II. Methods

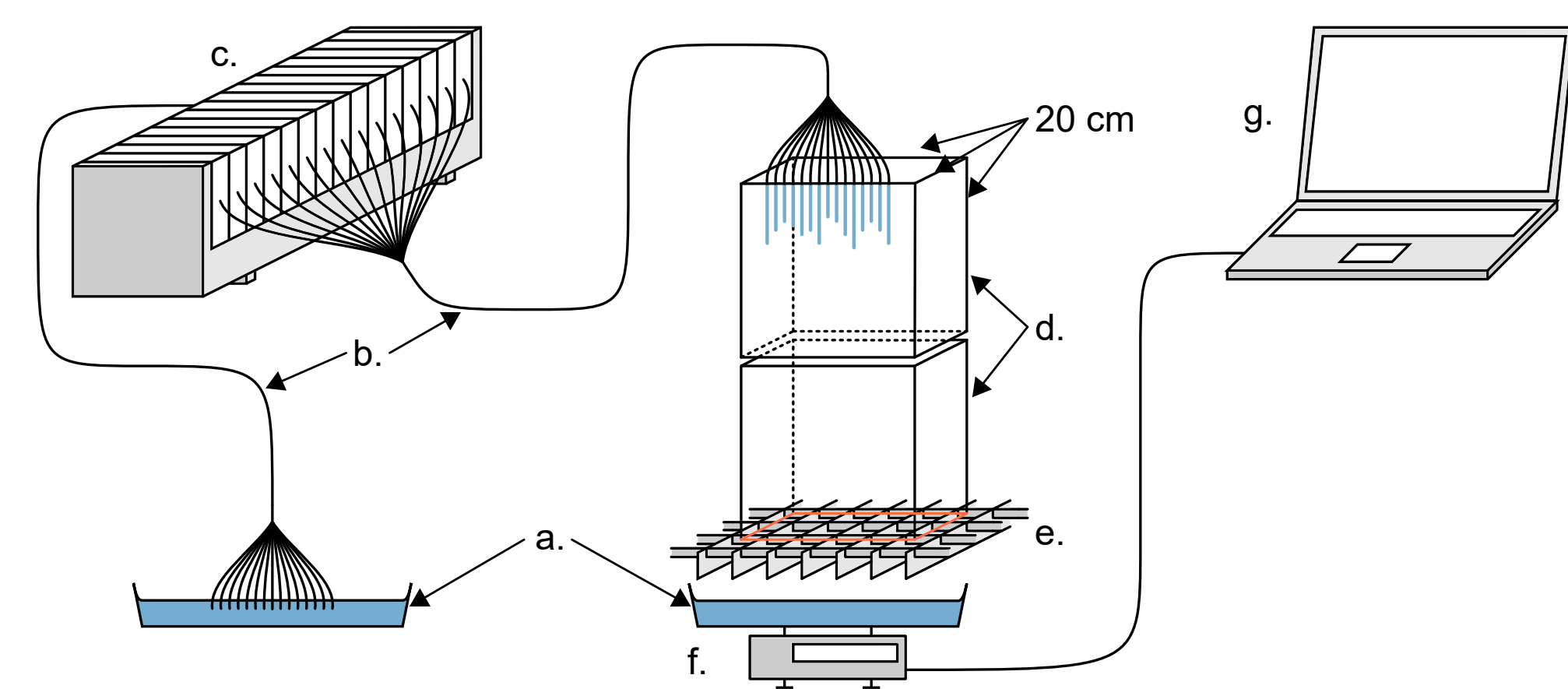


Figure 1: Experimental set-up: a. Water container, b. silicone tubes, c. multichannel dispenser, d. PMMA (poly(methyl methacrylate)) cube ($\theta_0 = (65.2 \pm 2.9)^\circ$), e. coated grate, f. digital balance, and g. computer

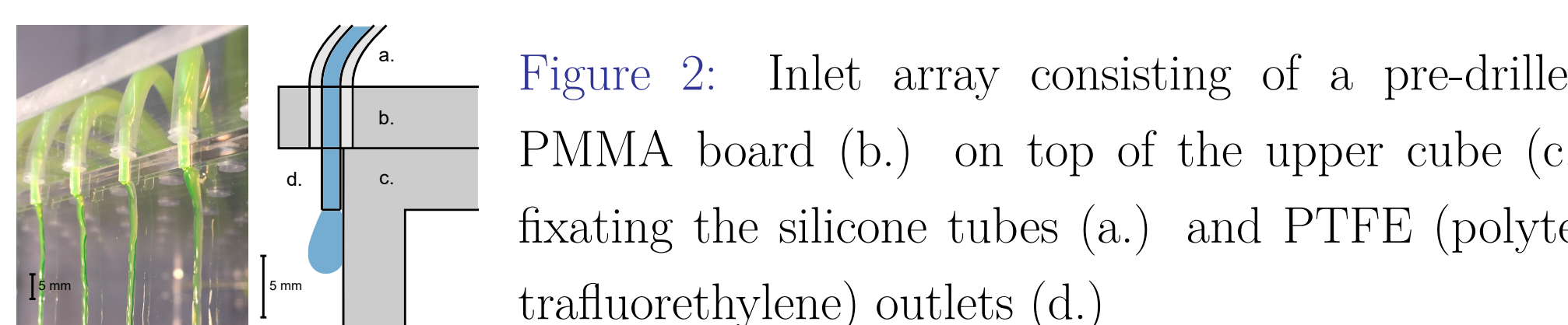


Figure 2: Inlet array consisting of a pre-drilled PMMA board (b.) on top of the upper cube (c.) fixing the silicone tubes (a.) and PTFE (polytetrafluorethylene) outlets (d.)

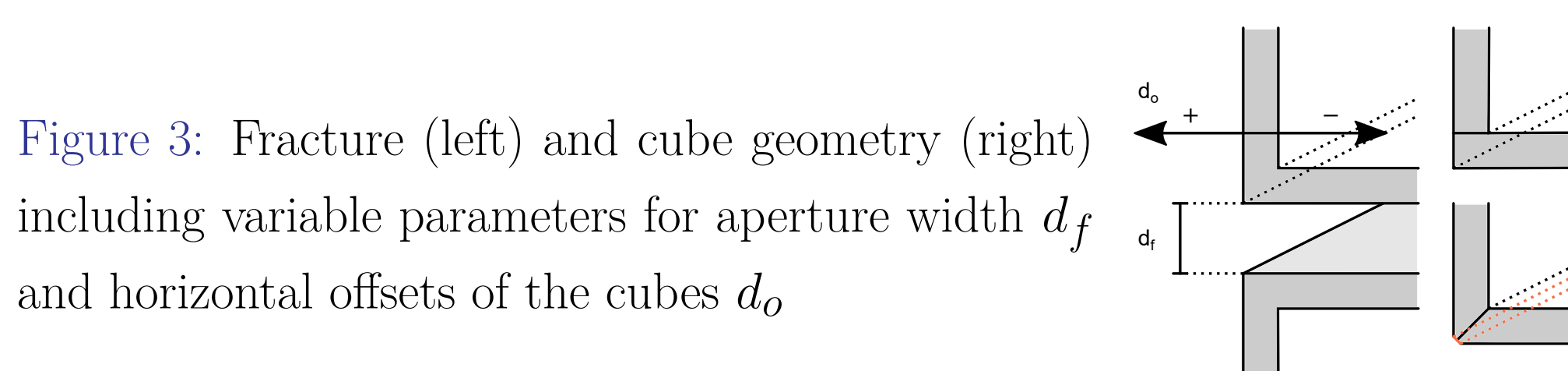


Figure 3: Fracture (left) and cube geometry (right) including variable parameters for aperture width d_f and horizontal offsets of the cubes d_o

III. Delineation of flow regimes

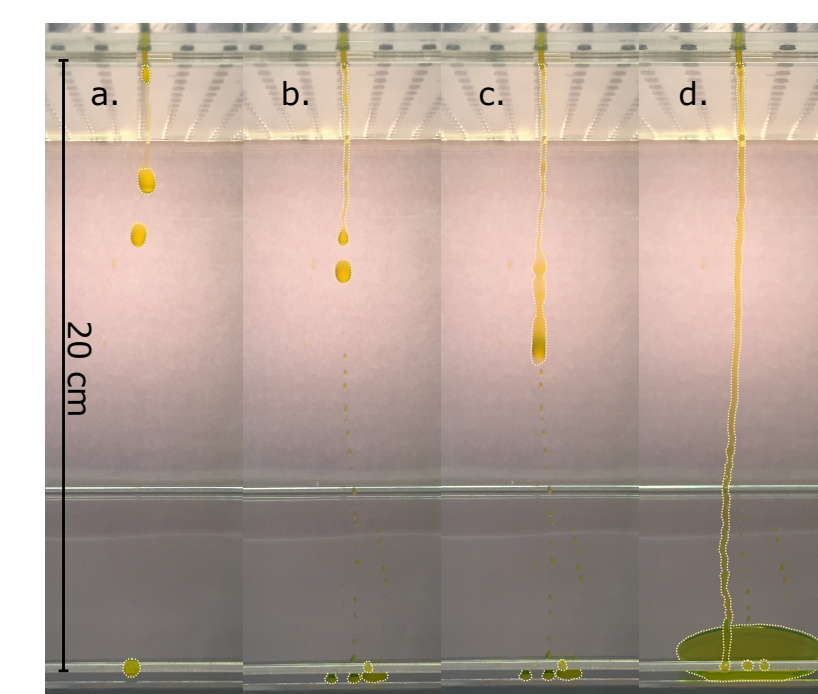


Figure 4: Free surface flow at $Q_0 = 1.5$ ml/min (a.), 2.5 ml/min (b.,c.), and 3 ml/min (d.).

- the transition is characterized by sliding drops and intermittent rivulets
- a high atm. pressure and temperature seemingly favours the stability of rivulet flow

Flow rate

- the volumetric flow rate Q_0 is varied to separate continuous droplet (≤ 1.5 ml/min) and rivulet flow (≥ 3 ml/min)

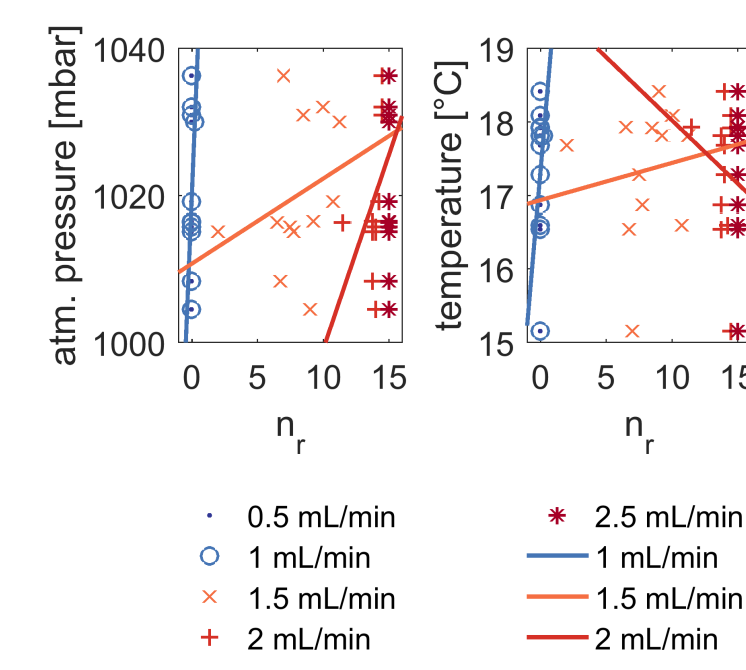


Figure 5: Atm. pressure and temperature vs. average number of stable rivulets n_r produced by 15 inlets. $R^2 = 0.08$ to 0.21 for displayed linear trends.

IV. Partitioning dynamics

1. Single-Inlet

- a sliding drop exhibits complex partitioning phenomena at unsaturated fracture intersections and either bypasses the aperture (a.) or contributes its complete or partial mass to the filling of the fracture (b.-f.)
- a rivulet establishes a hydraulic connection between inlet and fracture while effectively filling it (g.)

Figure 6: Partitioning dynamics at a horizontal fracture intersection captured at 240 fps.

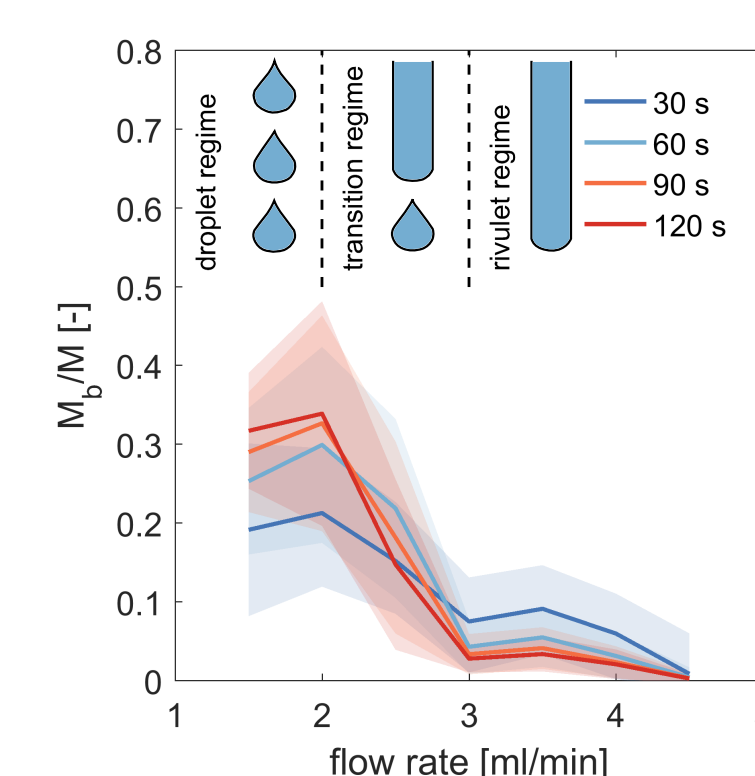
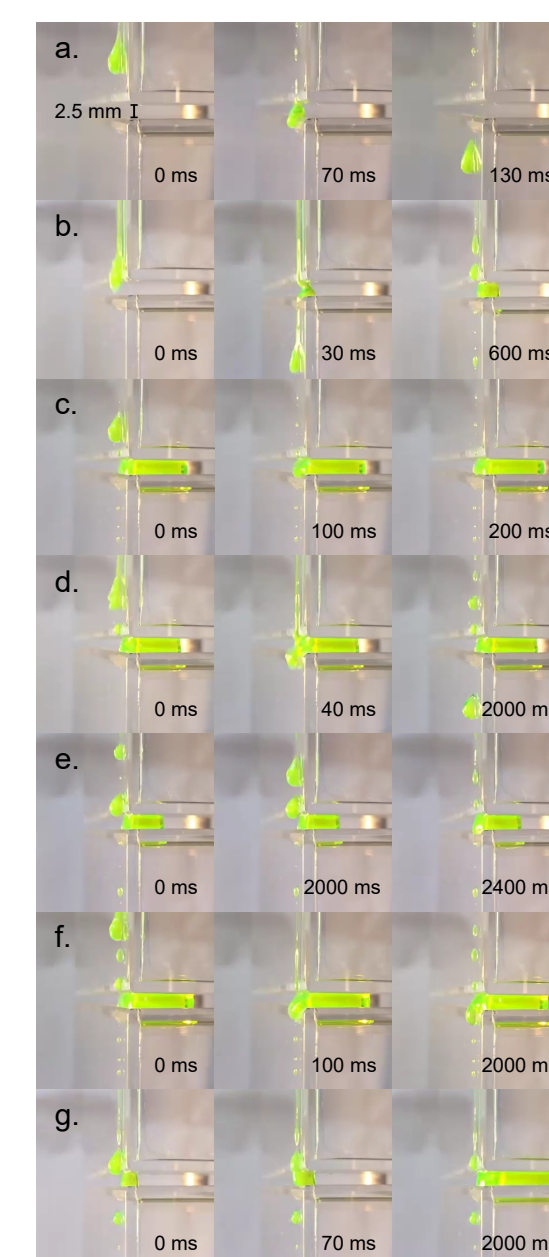


Figure 7: Average mass fractionation M_b/M vs. flow rate for $d_f = 2.5$ mm.

- the total liquid mass M can be calculated by

$$M(t) = Q_0 t, \quad (1)$$

where $Q_0 [L^3 T^{-1}]$ is the volumetric flow rate. The mass fractionation at time t is given by

$$M(t) = M_f(t) + M_b(t) \quad (2)$$

with M_f being the mass stored in the fracture and M_b representing the bypassing water.

IV. Partitioning dynamics (cont.)

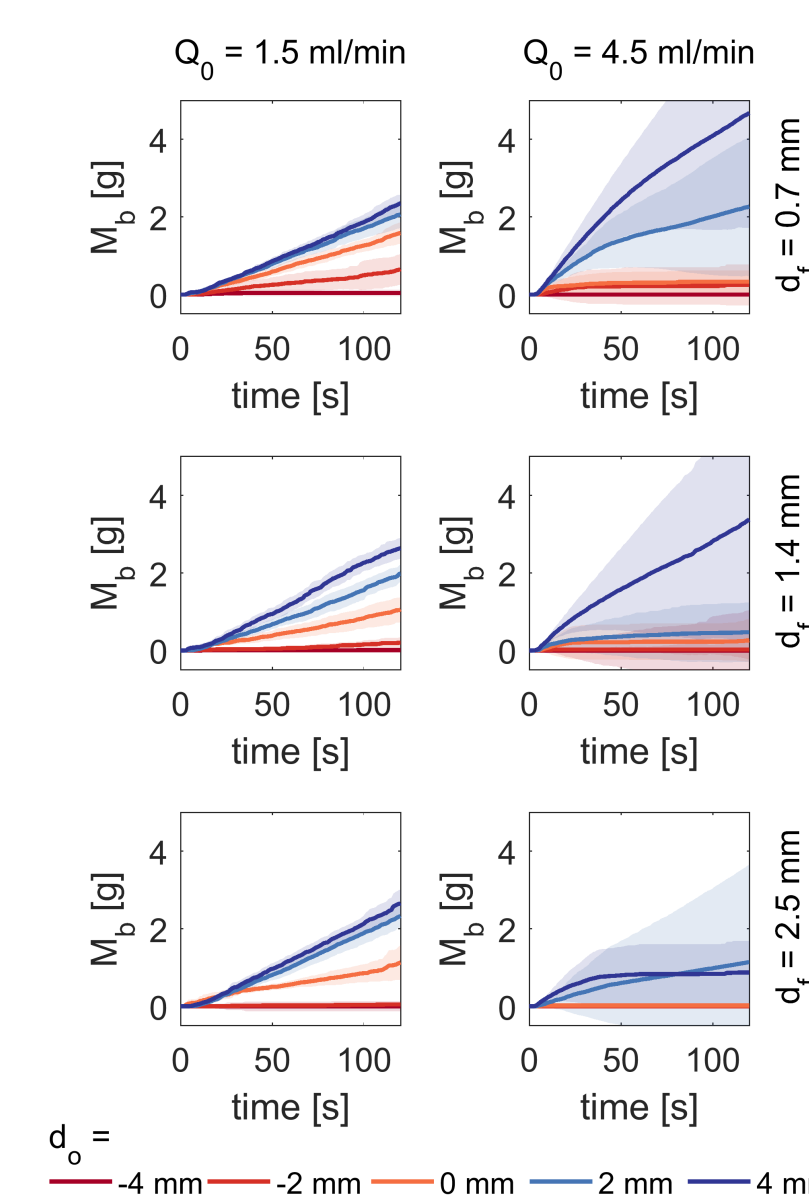


Figure 8: Average M_b vs. time for single-inlet experiments.

2. Multi-inlet

- equilibrium is reached where the fracture is fully saturated and Q_0 equals the discharge onto the drip pan; M_b rises linearly
- steady-state conditions are successively delayed as the number of fractures n_f and their respective aperture widths d_f increase
- hence, the disparity in bypass efficiency of droplet and rivulet flow is considerably large as long as unsaturated conditions are maintained

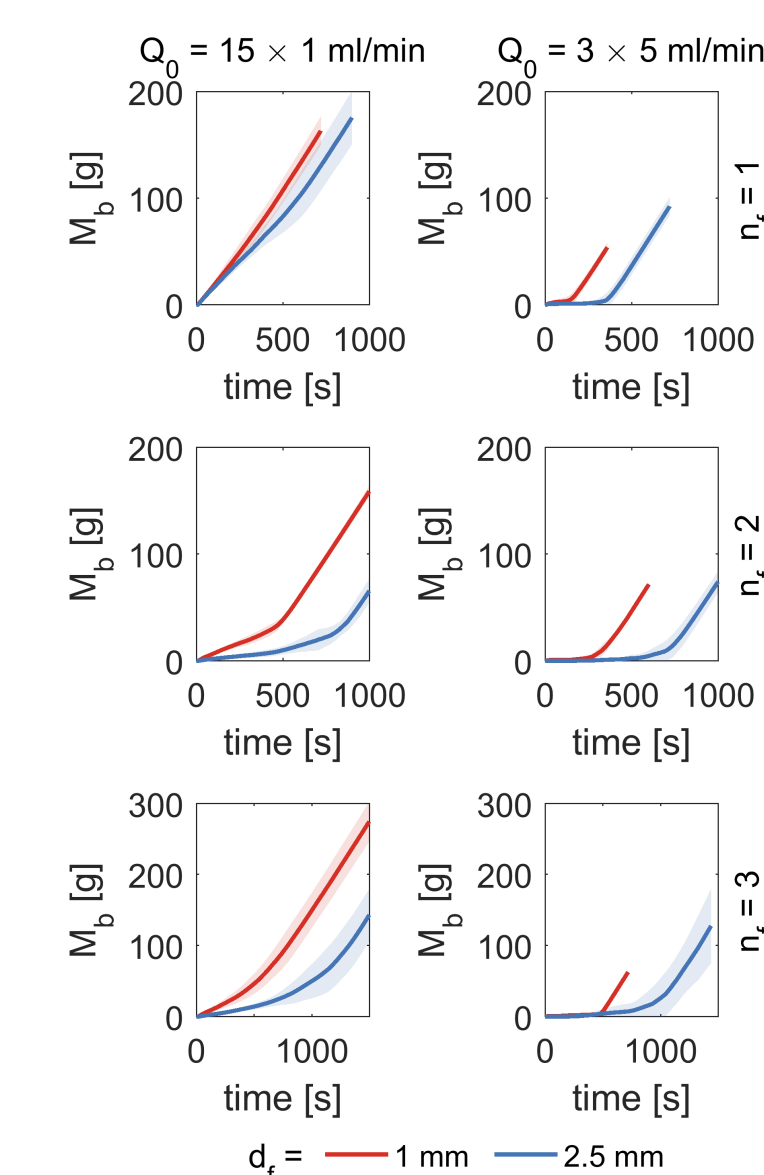


Figure 9: Ensemble means of M_b vs. time for multi-inlet experiments.

3. Washburn-type fracture inflow

- an analytical solution for capillary driven fracture inflow Q_f following Washburn (1921) is proposed by Kordilla et al. (2017):

$$\frac{dM(t)}{dt} = Q_0 = \frac{dM_f(t)}{dt} + \frac{dM_b(t)}{dt} \quad (3)$$

therefore, the volumetric fracture inflow rate is

$$Q_f(t) = \frac{dM_f(t)}{dt} = Q_0 - \frac{dM_b(t)}{dt} \quad (4)$$

The penetration length $l(t)$ is obtained by combining Poiseuille's law for planar fractures with an expression for the differential fluid volume in the element of $dl(t)$

$$\frac{dl(t)}{dt} = \frac{c_f}{l(t)} \quad (5)$$

where the constant c_f is

$$c_f = \frac{\Delta P_c d_f^2}{\mu \lambda} \quad (6)$$

with μ being the viscosity. The capillary pressure ΔP_c is given by

$$\Delta P_c = \frac{2\sigma \cos(\theta)}{d_f} \quad (7)$$

Figure 10: $Q_f(t)/Q_0$ and fitted eq. 9 for multi-inlet experiments

IV. Partitioning dynamics (cont.)

where σ represents the surface tension and θ being the contact angle. Solving eq. 5 for the initial length $l(t = t_0) = l_0$ gives

$$l(t) = \sqrt{l_0^2 + 2c_f(t - t_0)}. \quad (8)$$

The fluid mass within the fracture is $M_f(t) = A_f l(t)$ for a uniformly advancing front, where A_f is the cross-sectional area of the fracture aperture. Thus, the flow rate into the fracture according to eq. 4 is

$$Q_f(t) = A_f \frac{dl(t)}{dt} = \frac{Q_0}{\sqrt{1 + 2k_f(t - t_0)}} \quad (9)$$

with $A_f c_f = Q_0$ and $k_f = c_f/l_0$.

- parameters k_f and t_0 are adjusted in order to match the behaviour of eq. 9 with experimental results

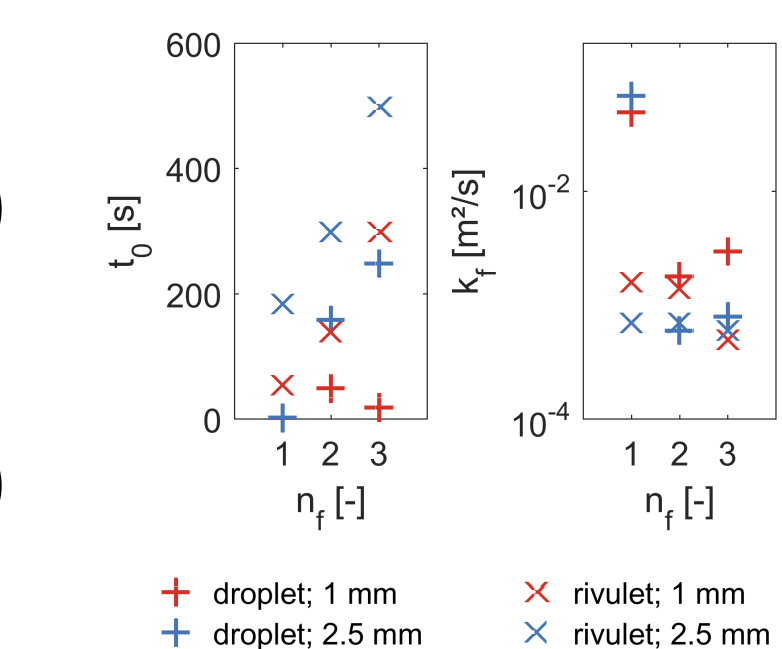


Figure 11: Adjusted parameters t_0 and k_f for eq. 9.

V. Conclusion

- free-surface flow exhibits complex partitioning dynamics at unsaturated fracture intersections with a considerably higher bypass efficiency of droplet flow
- variations of fracture geometry and the extent of the fracture cascade strongly influence the mass travel time distribution
- Washburn-type fracture inflow can be observed and reproduced for both flow regimes by an analytical solution

Outlook

- results will be applied to validate SPH (Smoothed Particle Hydrodynamics) models of gravity driven free-surface flow
- the proposed analytical solution fails to describe the inflow at an individual fracture in settings where $n_f > 1$ but rather approximates a mixed signature of simultaneously filling discontinuities
- hence, a memory function will be employed to reproduce the inflow at a selected fracture via rivulet flow and to possibly enable further upscaling:

We obtain $\varphi(t - t')$ in the sense of a memory function as

$$\varphi(t - t') = \frac{dQ_A^*(t)}{dt} \quad (10)$$

where

$$Q_A^*(t) = \frac{Q_A(t)}{Q_0} \quad (11)$$

is the normalized outflow rate from the system ($Q_0 = \text{const.}$), initially consisting of two cubes with one horizontal fracture. The volumetric outflow rate Q_A^* can then be obtained from

$$Q_A^* = \int_0^t \varphi(t - t') Q_A^*(t') dt' \quad (12)$$

Outflow from a second horizontal fracture, that is, for a system with three cubes can then be computed as

$$Q_A^* = \int_0^t \varphi(t - t') Q_A^*(t') dt' \quad (13)$$

hence, for a system consisting of n horizontal fractures we get

$$Q_A^* = \int_0^t \varphi(t - t') Q_A^{*n}(t') dt' \quad (14)$$

Acknowledgement:

This work was funded by the Deutsche Forschungsgemeinschaft (DFG; German Research Foundation) under grant no. SA 501/26-1 and KO 53591/1-1.

References:

- Washburn (1921): Phys. Rev. **(15(3))**; Towell & Rothfeld (1966): A.I.Ch.E. J. **(12(5))**; Schmucki & Laso (1990): J. of Fluid Mech. **(215)**; Dragila & Weisbrod (2003): Adv. in Water Res. **(26)**; Glass et al. (2003): Water Resour. Res. **(39)**; Dragila & Weisbrod (2004): Water Resour. Res. **(40)**; Ghezzehei (2004): Water Resour. Res. **(40)**; Ghezzehei (2005): Water Resour. Res. **(41)**; Nicholl & Glass (2005): Vad. Zone J. **(4)**; Nimmo (2012): Hydr. Proc. **26**; Kordilla et al. (2017): Water Resour. Res. **(53)**